THE JOURNAL OF BIOLOGICAL CHEMISTRY VOL. 290, NO. 41, pp. 25081–25089, October 9, 2015

The Cell Division Protein FtsZ from *Streptococcus pneumoniae* Exhibits a GTPase Activity Delay*

Received for publication, March 10, 2015, and in revised form, August 21, 2015 Published, JBC Papers in Press, September 1, 2015, DOI 10.1074/jbc.M115.650077

Estefanía Salvarelli[‡§1], Marcin Krupka[¶2], Germán Rivas[‖], Jesus Mingorance[‡], Paulino Gómez-Puertas[§], Carlos Alfonso[‖3], and Ana Isabel Rico[¶3]**

*From the [‡]Servicio de Microbiología, Hospital Universitario La Paz, IdiPAZ, 28046 Madrid, Spain, [§]Biomol-Informatics S.L., Universidad Autónoma, 28049 Madrid, Spain, the [¶]Centro Nacional de Biotecnología and the **Molecular Modelling Group, Centro de Biología Molecular "Severo Ochoa," Consejo Superior de Investigaciones Científicas, 28049 Madrid, Spain, and the [‖]Centro de Investigaciones Biológicas, Consejo Superior de Investigaciones Científicas, 28040 Madrid, Spain*

Background: The FtsZ cell division protein has nucleotide-dependent GTPase and assembly activities. The mechanism coupling these two activities is uncertain.
Results: Purified *Streptococcus pneumoniae* FtsZ (*Spn*FtsZ) presents a lag in the GTPase activity but not in filament assembly.
Conclusion: The differences between the initial polymerization and GTPase activities of *Spn*FtsZ suggest a transition from inactive to active polymers.
Significance: Nucleotide hydrolysis by *Spn*FtsZ polymers involves an activation step.

The cell division protein FtsZ assembles *in vitro* by a mechanism of cooperative association dependent on GTP, monovalent cations, and Mg^{2+}. We have analyzed the GTPase activity and assembly dynamics of *Streptococcus pneumoniae* FtsZ (*Spn*FtsZ). *Spn*FtsZ assembled in an apparently cooperative process, with a higher critical concentration than values reported for other FtsZ proteins. It sedimented in the presence of GTP as a high molecular mass polymer with a well defined size and tended to form double-stranded filaments in electron microscope preparations. GTPase activity depended on K^+ and Mg^{2+} and was inhibited by Na^+. GTP hydrolysis exhibited a delay that included a lag phase followed by a GTP hydrolysis activation step, until reaction reached the GTPase rate. The lag phase was not found in polymer assembly, suggesting a transition from an initial non-GTP-hydrolyzing polymer that switches to a GTP-hydrolyzing polymer, supporting models that explain FtsZ polymer cooperativity.

FtsZ is the main cytoskeletal protein involved in the division of most prokaryotes. The protein is generally considered the ancestor of tubulin, because it is a GTPase that polymerizes in a GTP-dependent manner (1), and they have a significant three-dimensional structure similarity (2, 3). Cell division begins with FtsZ localization and membrane anchoring, via other essential division proteins like FtsA, to form an annular structure at the division site termed the proto-ring (4–7). The ring is a dynamic structure that requires a constant energy input (8) and exchanges FtsZ monomers with a turnover of a few seconds (9). The proto-ring recruits the remaining essential division proteins to complete the divisome, the functional division machinery that exerts the force needed for cell constriction and conducts the biosynthesis of the septal cell wall (10–12). Because of its unique polymerization dynamics, FtsZ is also widely considered to have an active role in generating the motor force needed to pull the membrane and cell envelope inwards during cell division (13).

Escherichia coli FtsZ (*Ec*FtsZ), the most studied FtsZ protein, associates in the presence of GDP and Mg^{2+} following an isodesmic model to form short oligomers (14, 15). In the presence of GTP, Mg^{2+} and a monovalent cation (K^+, Na^+), *Ec*FtsZ assembles into long polymers of different lengths and structures, depending on the experimental conditions (16–19). Polymerization is very fast after GTP addition (20), rendering the kinetics of protein assembly particularly difficult to study. The existence of a critical protein concentration for assembly suggests a cooperative polymerization mechanism, but the details of the mechanism are not known (21–23). The dependence of protein assembly on Mg^{2+} concentration has been analyzed in the presence of constantly replenished GTP in steady state conditions using sedimentation velocity, concentration-gradient light scattering, fluorescence correlation spectroscopy, and dynamic light scattering, confirming the cooperative assembly of a narrow size distribution of fibrillar polymers with an average mass of 100 ± 20 FtsZ monomers (19, 24). Some models of cooperativity involve a nucleation step followed by protein conformational changes that would increase the affinity of the next monomer to be bound to the growing polymer (23, 25). In this way, the polymerization of *Mycobacterium tuberculosis* FtsZ (*Mtb*FtsZ) is also described as a cooperative assembly mechanism that involves a dimer nucleus, similar to *Ec*FtsZ, but with kinetics ~10 times slower (21). No structural evidence of nucleotide-dependent conformational changes has been found (26), although some have been proposed on the basis of analyses of tryptophan mutants and

* This work was supported in part by Spanish Government GrantsBIO2011-28941-C03 (to G. R. and C. A.) and BIO2011-28941-C01. The authors declare that they have no conflicts of interest with the contents of this article.
[1] Supported by Torres Quevedo Program Grant PTQ-11-05049 to Biomol Informatics S.L. To whom correspondence should be addressed: Servicio de Microbiología, Hospital Universitario La Paz, IdiPAZ, Paseo de La Castellana, 261, 28046 Madrid, Spain. E-mail: esalvarelli@gmail.com.
[2] Ph.D. fellow of the La Caixa Foundation International Fellowship Programme (La Caixa/CNB).
[3] Carlos Alfonso and Ana Isabel Rico are both senior authors.

molecular dynamics studies (27–29). An alternative model proposed an isodesmic growth cyclization process that would result in cooperativity (18, 30).

The *Streptococcus pneumoniae* FtsZ (*Spn*FtsZ) has not been characterized at the biochemical or biophysical level before. The protein was initially identified by Western blot analysis in *Streptococcus* cell extracts (31). More recently, FtsZ was quantified (3000 molecules/cell) and was shown to be essential for division (32); in immunostaining, it co-localized in cells with FtsA to form the midcell ring (33). Here we purified *Spn*FtsZ and analyzed its biochemical and functional properties, with emphasis on polymerization and GTPase activity, and compared them with *Ec*FtsZ.

Experimental Procedures

SpnFtsZ Gene Cloning—Standard protocols for molecular cloning, transformation, and DNA analysis were as described (34). Plasmids encoding the streptococcal FtsZ protein for overproduction and purification were obtained by subcloning the *ftsZ* gene from the pBAD-FtsZ vector (kindly provided by Dr. Orietta Massidda, University of Cagliari, Cagliari, Italy). Primers MK14 (5′-GGGATCCCATATGACATTTTCATTTGATACAGC-3′) and MK15 (5′-CGGAATTCTTAACGATTTTTTGAAAAATGG-3′) (Sigma-Aldrich) were used to amplify the *ftsZ* gene sequence. This gene was inserted into the NdeI-EcoRI restriction sites of the overexpression vector pET24a (Invitrogen), yielding the plasmid pMKV18, which encodes the *Spn*FtsZ protein without the His tag. Correct gene cloning was confirmed by DNA sequencing.

SpnFtsZ Purification—To purify *Spn*FtsZ, *E. coli* C41 cells transformed with plasmid pMKV18 were grown (2 h, 37 °C) in 2 liters of Luria broth supplemented with kanamycin (50 μg ml^{-1}). At an A_{600} of 0.45, *Spn*FtsZ overproduction was induced for 3 h by addition of 1 mM isopropyl-1-thio-β-D-galactopyranoside. Cells were harvested by centrifugation (5,000 $\times$ *g*, 20 min, 4 °C), resuspended in 40 ml of PEM buffer (50 mM PIPES, pH 6.5, 1 mM EDTA, 5 mM $MgCl_2$), and frozen at −80 °C. Cells were lysed by sonication, and the soluble fraction containing *Spn*FtsZ was purified by Ca^{2+}-induced precipitation (15). Briefly, the lysate was cleared by centrifugation (50,000 $\times$ *g*, 30 min at 4 °C), and then GTP and $CaCl_2$ were added to the supernatant to 1 and 20 mM final concentrations, respectively. The mixture was incubated 15 min at 30 °C and centrifuged (30,000 $\times$ *g*, 15 min at 4 °C). The pellet containing FtsZ was resuspended again in PEM buffer, cleared by centrifugation (30,000 $\times$ *g*, 15 min at 4 °C), and the supernatant was subjected to another cycle with GTP and $CaCl_2$. The pelleted protein was resuspended in 50 mM Tris-HCl, pH 8.0, 0.1 mM EDTA, 5 mM $MgCl_2$, and loaded into a HiTrap Q FF column in an ÄKTAprime plus system (GE Healthcare) equilibrated in the same buffer. The column was washed with the equilibration buffer and next with a 0–1 M gradient of KCl in buffer. The protein eluted in a range of 300–400 mM KCl, fractions were pooled and dialyzed against 50 mM Tris-HCl, pH 7.5, 5 mM $MgCl_2$, 300 mM KCl. Protein purity was confirmed by SDS-PAGE.

Protein Identification by Peptide Footprint—As *Spn*FtsZ showed a higher relative molecular mass than predicted, and the protein sequence was confirmed by mass spectrometry analysis of peptides produced by proteolysis. Trypsin-digested samples were analyzed with an Autoflex III TOF/TOF mass spectrometer (Bruker-Daltonics). MALDI-MS and MS/MS data were combined through the BioTools 3.0 program (Bruker-Daltonics), and MASCOT software 2.3 (Matrix Science) was used for amino acid sequence analysis with NCBI nonredundant protein database (accession number 20100306). Protein scores >86 were considered as being significant ($p < 0.05$) (35).

Determination of Protein Concentration—Because *Ec*FtsZ purified by the same method as *Spn*FtsZ bears a GDP molecule and protein absorbance at 280 nm is affected by the nucleotide (15), we calculated protein concentration using the Bradford colorimetric assay (Bio-Rad) and BSA as reference (*Spn*FtsZ and BSA produced identical color in the colorimetric assay). This method reproducibly estimates *Spn*FtsZ concentration, as confirmed by quantitative amino acid analysis (36). GDP content was estimated by protein precipitation with 10% (v/v) perchloric acid as described (15).

Analysis of FtsZ Polymerization by Static Light Scattering—*Spn*FtsZ or *Ec*FtsZ proteins were diluted to desired concentrations in polymerization buffer (50 mM Tris-HCl, pH 7.5, 250 mM KCl, 5 mM $MgCl_2$). Five seconds after addition of 1 mM GTP, FtsZ polymer formation was monitored by 90° light scattering measurement at 24 °C on a Hitachi F-2500 fluorescence spectrophotometer. Excitation and emission wavelengths were set to 320 nm with 5-nm slit widths, as described (20).

Electron Microscopy—To observe *Spn*FtsZ polymer morphology, the polymerization reaction described above was terminated at 4 min, and samples were adsorbed on a 400-mesh collodion-coated, glow-discharged copper grid for 1 min, negatively stained with 2% (w/v) uranyl acetate, then imaged with a Jeol JEM1011 transmission electron microscope, and photographed with an 11 megapixel charge-coupled device camera (Gatan Erlangshen ES1000W). Images were captured with Gatan Digital Micrograph 1.8.0 software and processed with Adobe Photoshop CS5. FtsZ polymer length and width were measured using the public image analysis program Object-Image. Approximately 100 polymers were analyzed for length, and 50 paired filaments were analyzed for width.

Analytical Centrifugation—Sedimentation velocity experiments were performed in an Optima XL-I ultracentrifuge (Beckman Coulter) equipped with absorbance and interference optics to monitor *Spn*FtsZ sedimentation in the presence of 1 mM nucleotide (GDP or GTP). Various concentrations of *Spn*FtsZ were equilibrated in polymerization buffer and immediately before sedimentation, and *Spn*FtsZ samples were supplemented with 1 mM GDP or GTP and centrifuged (30,000-48,000 rpm, 20 °C) in an An50Ti eight-hole rotor and double-sector Epon-charcoal centerpieces. For polymer formation with GTP, a GTP regeneration system (GTP/RS, containing acetate kinase and acetyl phosphate) was added to avoid complete GTP depletion during data collection in sedimentation velocity analysis (37). Elapsed time between GTP/RS addition and the last scan used in data analysis was adjusted for optimal visualization of GTP-*Spn*FtsZ polymers in solution (polymers were stable for ~50 min). Differential sedimentation coeffi-

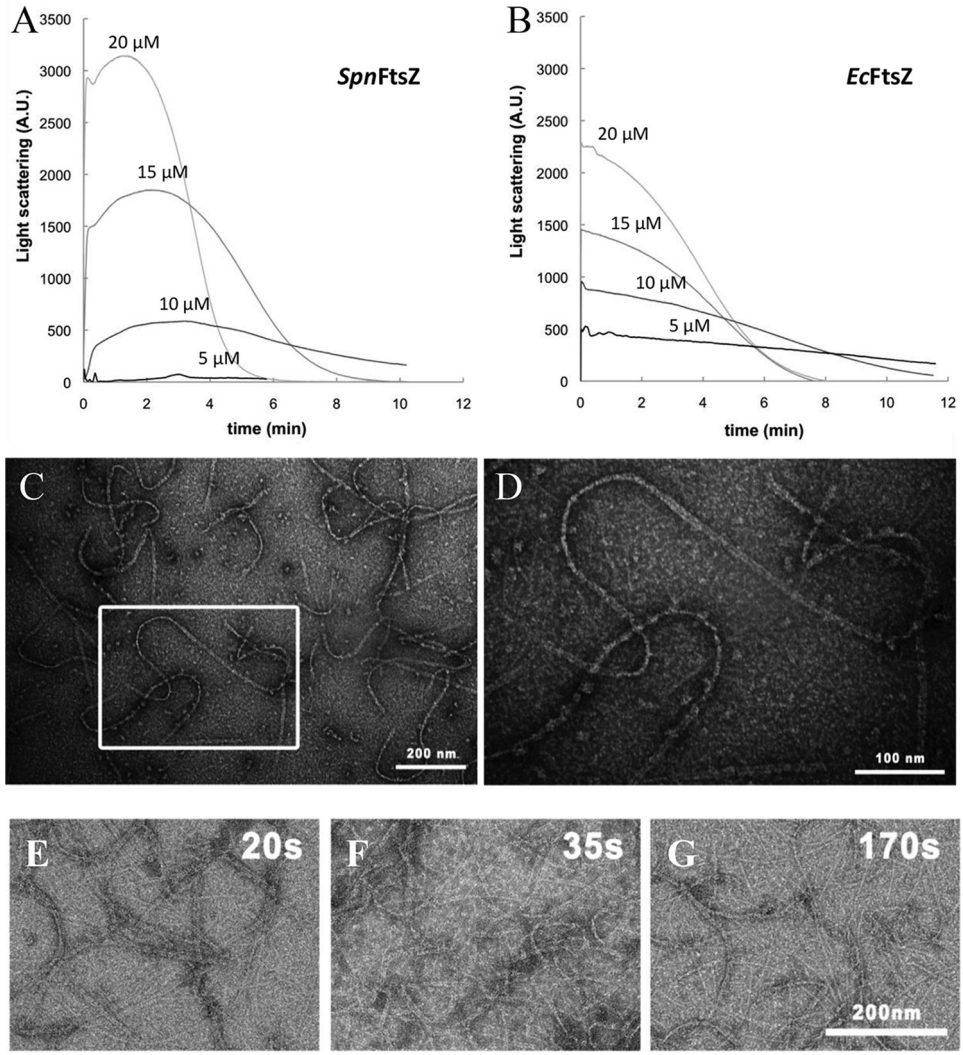

FIGURE 1. ***Spn*FtsZ polymerization.** *A* and *B*, polymer formation in polymerization buffer (50 mM Tris-HCl, pH 7.5, 250 mM KCl, 5 mM $MgCl_2$) was followed by 90° light scattering after addition of 1 mM GTP. *Curves* (*black* to *light gray*) correspond to 5, 10, 15, and 20 μM, respectively, as indicated, for *Spn*FtsZ (*A*) and *Ec*FtsZ (*B*). Times to maximum assembly after GTP addition were calculated from *Spn*FtsZ profiles: 3.1 min for 10 μM (I_{max} = 560 AU), 2.0 min for 15 μM (1687 AU), and 1.3 min for 20 μM (3025 AU). *C*, polymers obtained in 4 min with 10 μM *Spn*FtsZ, as described under "Experimental Procedures," were analyzed by electron microscopy. *D*, amplified image of a polymer. *E–G* show polymers obtained at 20, 35, and 170 s, respectively (included 20 s of adsorption time), with 15 μM *Spn*FtsZ.

cient distribution $c(s)$ was calculated by least squares boundary modeling of the experimental data using the SEDFIT program (38). The s values were corrected to standard conditions using SEDNTERP software, yielding standard s values ($s_{20,w}$).

To determine the oligomerization state of *Spn*FtsZ in the presence of GDP, short column (85 μl) sedimentation equilibrium of the *Spn*FtsZ samples, alone or with 0.1 mM GDP, was performed at multiple speeds (9,000, 13,000, and 18,000 rpm). Following equilibrium scans, high speed centrifugation analysis (48,000 rpm) was used to estimate the baseline offsets. Weight average buoyant molecular weight was determined by fitting a single species model to the experimental data using the HETEROANALYSIS program (39).

Dynamic Light Scattering—Dynamic light scattering experiments were carried out in a Protein Solutions DynaPro MS/X instrument (Protein Solutions) at 20 °C, as described (19). The data were analyzed using MATLAB (version 7.0.4; MathWorks). Correlation functions for mono- and polydisperse particles were analyzed to calculate translation diffusion coefficient values, D_t (19). The apparent molar mass of polymers was calculated according to the Svedberg equation using the average of the standard translation diffusion coefficient values D obtained by dynamic light scattering and the average $s_{20,w}$ (s values corrected to standard conditions of water, 20 °C, and infinite dilution) obtained from analysis of independent sedimentation velocity profiles (24).

GTPase Activity—FtsZ GTPase activity was determined by the malachite green method (40). Hydrolysis reactions were performed as described above in polymerization buffer at 24 °C with 1 mM GTP. Samples were collected at various times and diluted in the same buffer containing 65 mM EDTA to terminate the reaction. Malachite green-molybdate reagent was added, and absorbance was measured at 620 nm. Phosphate concentrations were calculated from a Na_2HPO_4 standard curve, and the GTPase activity reaction rate (V, molP/molFtsZ/min) was determined from the slope of the linear part of phos-

phate accumulation curves. To determine the activation delay of the GTP hydrolysis, the curves were divided in two sections, and linear regression was done independently for each section. The delay of the GTP hydrolysis was calculated from the crossing point between the two regression lines. Enzymatic parameters (K_m and V_{max}) were calculated from the kinetic curves using GraphPad Prism 5.0. All reactions were performed in duplicate.

Results and Discussion

In this study we have purified and characterized the wild-type FtsZ protein from *S. pneumoniae* (*Spn*FtsZ) and compared its biochemical and assembly properties with those of *E. coli* (*Ec*FtsZ), the best studied FtsZ protein.

Functional Properties of Purified SpnFtsZ—*Spn*FtsZ was overproduced in *E. coli* cells and purified at high yield (40 ± 10 mg of protein per liter of culture) in native conditions using cycles of Ca^{2+}-induced protein precipitation as previously described for *Ec*FtsZ purification (15). Electrophoretic analysis of the purified protein showed a single band corresponding to a relative mass of 49,490 ± 900 Da (data not shown), a value slightly higher than that predicted from the amino acid sequence (44,416 Da), that lead to confirm by peptide mass fingerprinting that the protein sequence of the purified protein was the one expected. Purified *Spn*FtsZ has 0.7 ± 0.1 mol of bound GDP per mol of protein monomer.

*Spn*FtsZ polymerization was triggered with GTP, in 250 mM KCl, 5 mM $MgCl_2$ in 50 mM Tris-HCl, pH 7.4 (polymerization buffer) and was monitored at 24 °C by light scattering (Fig. 1*A*). The signal caused by polymer formation increased over 1–3 min before reaching the maximum level of polymerization. The reaction was faster for the highest protein concentration assayed (1 min for 20 μM *Spn*FtsZ, 3 min for 10 μM). Polymers disassembled after a few minutes. No assembly was observed at 5 μM *Spn*FtsZ. On the other hand, the polymers of *Ec*FtsZ monitored in conditions identical to those of *Spn*FtsZ reached their maximum polymerization signal inmediately at any protein concentration assayed (5–20 μM *Ec*FtsZ) (Fig. 1*B*).

The *Spn*FtsZ polymers consisted of single- and double-stranded filaments, the latter being predominant, with a narrow size distribution (10 ± 1 nm, 540 ± 200 nm) as revealed by negative stain electron microscopy (Fig. 1, *C* and *D*). There are no qualitative differences in the structure of the polymers at the beginning of the reaction (Fig. 1, *E*–*G*) as shown in the images obtained at shorter times (20, 35, and 170 s respectively). Under similar polymerization conditions, *Ec*FtsZ preparations showed individual filaments and up to 3–4 lateral associated filaments, as reported (1, 23, 41, 42). Preferentially double filaments were also observed in *M. tuberculosis* FtsZ (*Mtb*FtsZ) preparations at pH 6.5 (not at pH 7.7) (21) and in the thermophilic *Methanococcus jannaschii* FtsZ (*Mj*FtsZ) at pH 6.5 at 55 °C (43).

The GDP Form of SpnFtsZ Does Not Oligomerize in the Presence of Magnesium—The association state of the GDP form of purified *Spn*FtsZ, and its possible modulation by Mg^{2+} and protein levels, as in the case of *Ec*FtsZ (15, 24), were measured by analytical ultracentrifugation. In sedimentation velocity experiments, at the highest protein concentration tested (25 μM), *Spn*FtsZ sedimented as a main single homogeneous species, corresponding to 80–95% of total protein, with a sedimentation coeficient value of 2.9 ± 0.1 S in the presence of 1 mM GDP, independently of Mg^{2+} concentration (from EDTA to 5 mM $MgCl_2$) (Fig. 2*A*). This species is compatible with *Spn*FtsZ protein monomers, as confirmed by the sedimentation equilibrium analysis (Fig. 2*B*). From these experiments, we conclude that the GDP form of *Spn*FtsZ is a monomer with an overall structure that slightly deviates from the globular shape (frictional ratio = 1.5–1.6) which, unlike *Ec*FtsZ (15), does not have a tendency to form oligomers in the presence of Mg^{2+}.

The GTP Polymer of SpnFtsZ Is Larger than That of EcFtsZ—*Spn*FtsZ polymerization driven by GTP was analyzed at steady state by sedimentation velocity in the presence of a GTP-regen-

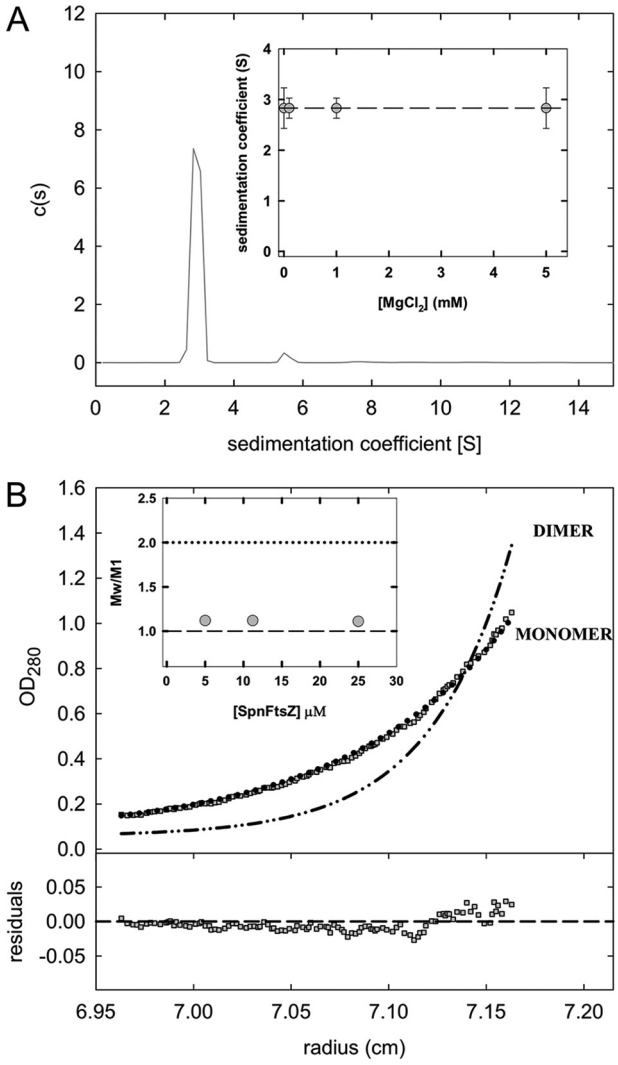

FIGURE 2. ***Spn*FtsZ association in the presence of GDP/Mg^{2+}.** *A*, velocity sedimentation analysis. Sedimentation coefficient distribution using 25 μM *Spn*FtsZ and 1 mM GDP in 50 mM Tris-HCl, pH 7.5, 250 mM KCl with 1 mM $MgCl_2$ concentration. The *inset* represents sedimentation coefficient variation of the main sedimenting species with increasing $MgCl_2$ concentrations: from 0.1 to 5 mM (first value corresponds to 0.1 mM $MgCl_2$ supplemented with 2 mM EDTA). *B*, sedimentation equilibrium analysis. *Spn*FtsZ gradient in polymerization buffer (containing 5 mM $MgCl_2$) with 0.1 mM GDP (18,000 rpm; 20 °C). *Gray squares*, experimental data; *dotted line*, theoretical gradient for the *Spn*FtsZ monomer (44,416 Da); *dotted* and *dashed line*, theoretical gradient for the *Spn*FtsZ dimer (88,832 Da). The *inset* represents the variation of the association state of *Spn*FtsZ with protein concentration.

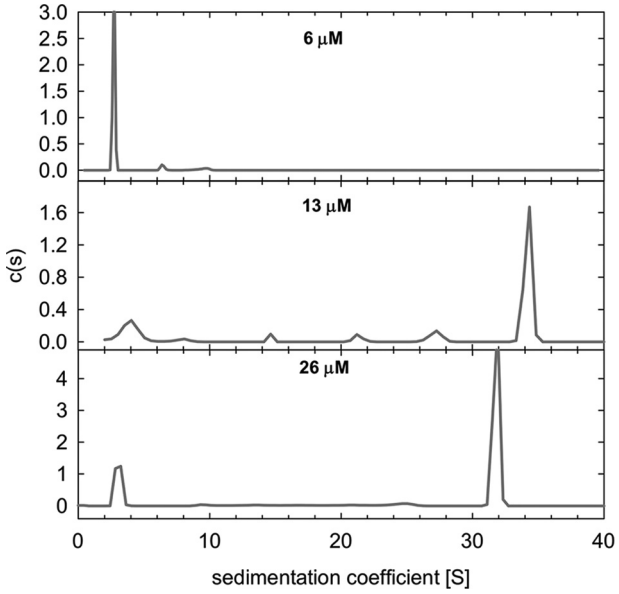

FIGURE 3. **Sedimentation velocity analysis of *Spn*FtsZ polymer.** Sedimentation coefficient distributions of three concentrations of *Spn*FtsZ in polymerization buffer supplemented with 1 mM GTP, in a GTP regeneration system.

erating system as previously done with the FtsZ protein from *E. coli* (18, 30, 44). In accordance with the light scattering measurements, no assembly of *Spn*FtsZ was detected at low protein concentration (6 μM), and the protein was distributed as slowly sedimenting species with a *s* value corresponding to the monomeric species (~3.0 S) (Fig. 3). At higher concentrations, most of the protein was found as a rapidly sedimenting fraction with an average sedimentation coefficient of 34 ± 3 S ($s_{20,w}$). This fraction represents a narrow sized distribution, resembling thus the sedimentation behavior of *Ec*FtsZ (18, 30, 44). However, the *s* value of the rapid sedimenting species of *Spn*FtsZ is much higher than the one of the *Ec*FtsZ polymeric species, suggesting that the average size of the protofilaments of *Spn*FtsZ is higher as well (18). Dynamic light scattering was then used to measure the diffusion coefficient of the rapid sedimenting species of *Spn*FtsZ (2.1 ± 0.1 $\mu m^2\ s^{-1}$). From the measured *s* and D values, following the Svedberg equation, the average molar mass of the polymeric species was found to be 320 ± 25 monomers per protofilament, three times higher than the number of FtsZ subunits forming the protofilament in *E. coli* (100 ± 20 monomers) under similar experimental conditions (30, 44).

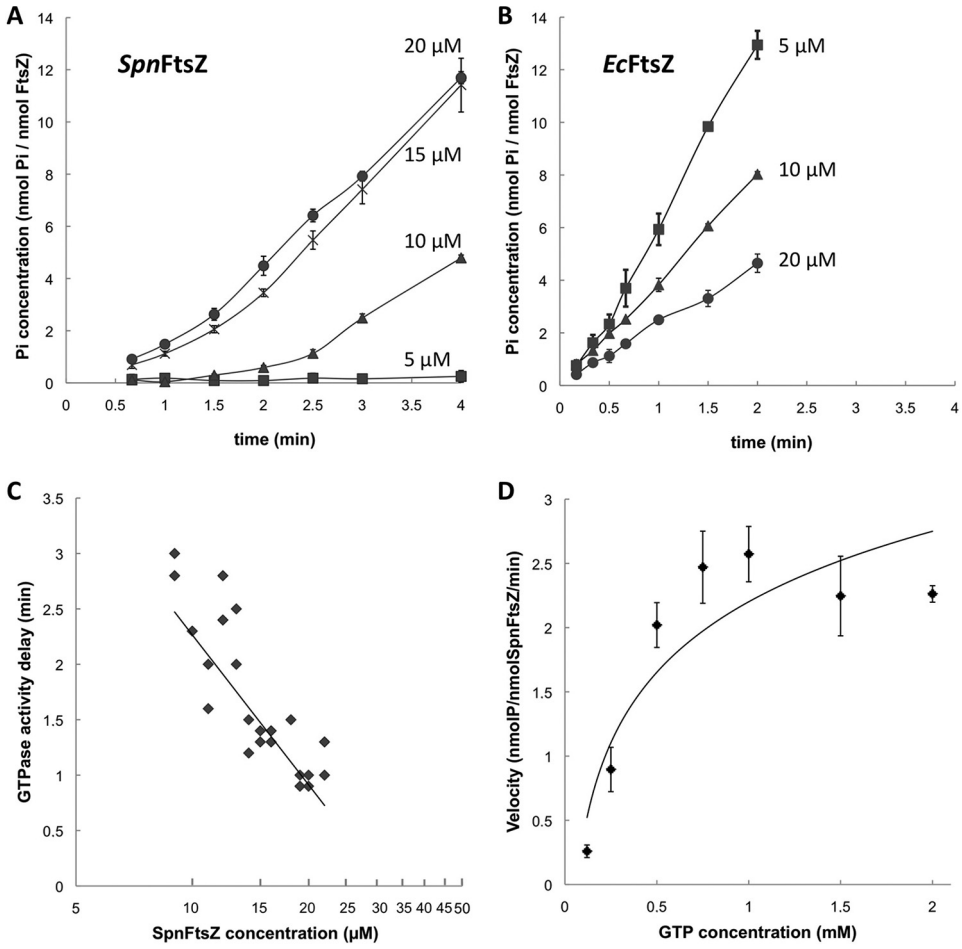

FIGURE 4. **GTPase activity of *Spn*FtsZ.** Protein samples were incubated with 1 mM GTP in polymerization buffer. *A* and *B*, phosphate accumulation curves produced by *Spn*FtsZ (*A*) and *Ec*FtsZ (*B*) were determined by duplicates at various protein concentrations (*squares*, 5 μM; *triangles*, 10 μM; *crosses*, 15 μM; *circles*, 20 μM). *Error bars* are drawn. *C*, GTPase activity delay, calculated as the time corresponding to the intersection value of the two regression lines determined in the phosphate accumulation curves obtained for a *Spn*FtsZ concentration, semi-log plotted against protein concentrations ($p < 0.001$, $n = 26$ independent experiments). *D*, increasing GTP amounts were incubated with 15 μM *Spn*FtsZ in polymerization buffer. Velocities were obtained from the slopes of the phosphate accumulation curves and fitted to a Michaelis-Menten model with $V_{max} = 3.3$ nmol GTP/nmol FtsZ/min and $K_m = 430$ μM ($n = 20$ independent experiments).

GTPase Activity of SpnFtsZ: an Activation Delay of the GTP Hydrolysis—At 5 μM *Spn*FtsZ, the protein did not hydrolyze GTP, in agreement with the absence of polymerization (Fig. 4*A*). At the threshold concentration for assembly (10 μM), the GTPase activity had a lag (1.5 min), during which there was polymerization but no phosphate accumulation. Then GTPase activity increased to a rate of 2.43 ± 0.02 molP/mol*Spn*FtsZ/min. The activation delay of the GTP hydrolysis (lag plus transition phase) was strongly dependent on protein concentration, being shorter as *Spn*FtsZ concentration increased. The delays to attain the GTPase reaction rate calculated for 10, 15, and 20 μM *Spn*FtsZ were 2.4, 1.6, and 1.0 min, respectively (Fig. 4*C*). Reaction rates were similar at 15 μM *Spn*FtsZ (3.80 ± 0.42 molP/mol*Spn*FtsZ/min) and 20 μM *Spn*FtsZ (3.60 ± 0.07 at 20 μM).

This behavior differed from that of *Ec*FtsZ, for which no activation delay of the GTP hydrolysis was detected in same experimental conditions, even approximately at its critical assembly concentration (Fig. 4*B*). In addition, *Ec*FtsZ GTPase activity reached its maximal rate at 5 μM protein (V = 6.76 ± 0.16 molP/mol*Ec*FtsZ/min), with a progressive decrease at higher concentrations (3.99 ± 0.06 at 10 μM and 2.26 ± 0.16 at 20 μM), in accordance with our previous reported data (45). An activation delay of the GTP hydrolysis has been described for *Staphylococcus aureus* FtsZ (*Sa*FtsZ) that hydrolyzes GTP above 4 μM protein after a transition phase that was shorter as the protein concentrations increased (46).

GTPase Kinetics of SpnFtsZ—To evaluate *Spn*FtsZ GTPase activity kinetics, different GTP concentrations were hydrolyzed with a saturated amount of *Spn*FtsZ (15 μM) in polymerization buffer. Velocities of the GTP hydrolysis fitted to a Michaelis-Menten kinetic model (Fig. 4*D*), with V_{max} = 3.3 ± 0.4 nmolP/nmolFtsZ/min, and K_m = 430 ± 138 μM. Velocity of GTP hydrolysis was 2-fold lower than that reported for *Ec*FtsZ, calculated in the same experimental conditions (V_{max} = 6 nmolP/nmolFtsZ/min, K_m = 300 μM) (47). On the other hand, *Mt*FtsZ kinetic was described 10-fold slower than *Ec*FtsZ (at pH 7.7, room temperature) (21) as well as *Sa*FtsZ, with a lower GTP hydrolysis rate (~1.0 min^{-1} at pH 6.5, 30 °C) (46), whereas *Mj*FtsZ showed similar kinetic values as the *E. coli* protein (~5.9 min^{-1} at pH 6.5, 55 °C) at its optimal conditions (43).

Cation Dependence of the GTPase Activity of SpnFtsZ—The GTPase activity of FtsZ from *E. coli* and other species depends on cation binding (48). We assayed *Spn*FtsZ GTP hydrolysis at different K^+, Mg^{2+}, and Na^+ concentrations and compared with *Ec*FtsZ values in the same conditions (1 mM GTP and standard salt concentrations except that tested). *Spn*FtsZ required at least 100 mM KCl to start to hydrolyze GTP, and the reaction rate reached a maximum at 200 mM KCl (Fig. 5*A*). In contrast, *Ec*FtsZ reached a maximum at 100 mM KCl, which was maintained at higher K^+ concentrations. *Spn*FtsZ did not hydrolyze GTP at 1 mM $MgCl_2$ and needed 3 mM $MgCl_2$ for optimal activity; *Ec*FtsZ showed 80% of its maximum GTPase rate at 1 mM $MgCl_2$ (Fig. 5*B*). GTP hydrolysis by *Spn*FtsZ decreased when increasing amounts of NaCl were present in the GTPase reaction, and it was completely inhibited at 250 mM NaCl (Fig. 5*C*). *Ec*FtsZ activity showed no GTPase inhibition, even at 500 mM NaCl. In summary, *Spn*-

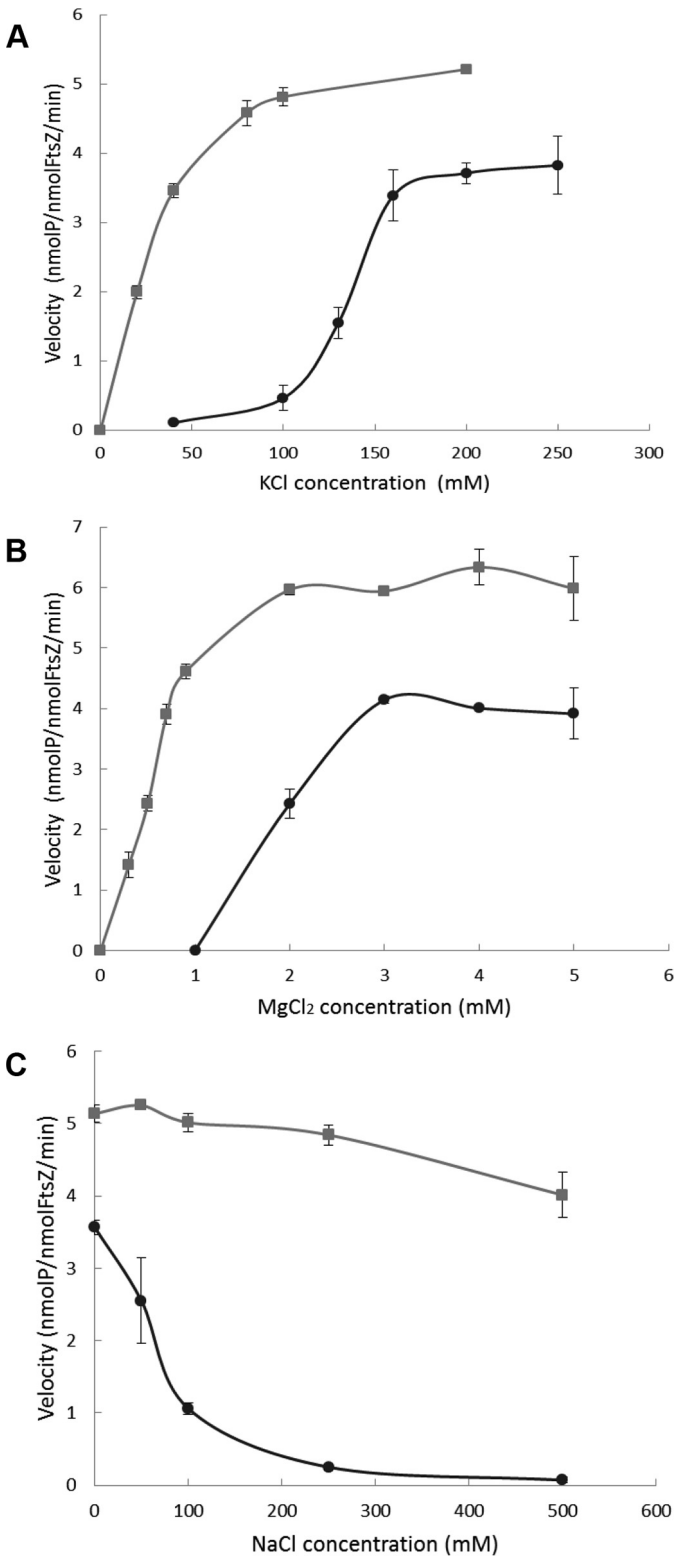

FIGURE 5. **Cation dependence of *Spn*FtsZ GTPase activity.** Hydrolysis of GTP (1 mM) was measured in polymerization buffer modified with different salt concentrations. *A*, 5 mM $MgCl_2$, with different KCl concentrations. *B*, 250 mM KCl, with varied $MgCl_2$ concentrations. *C*, 5 mM $MgCl_2$, 250 mM KCl, plus different NaCl concentrations. *Black circles* correspond to the velocity values calculated from the phosphate accumulation *curves* of *Spn*FtsZ (10 μM) and *gray squares* from those for *Ec*FtsZ (10 μM).

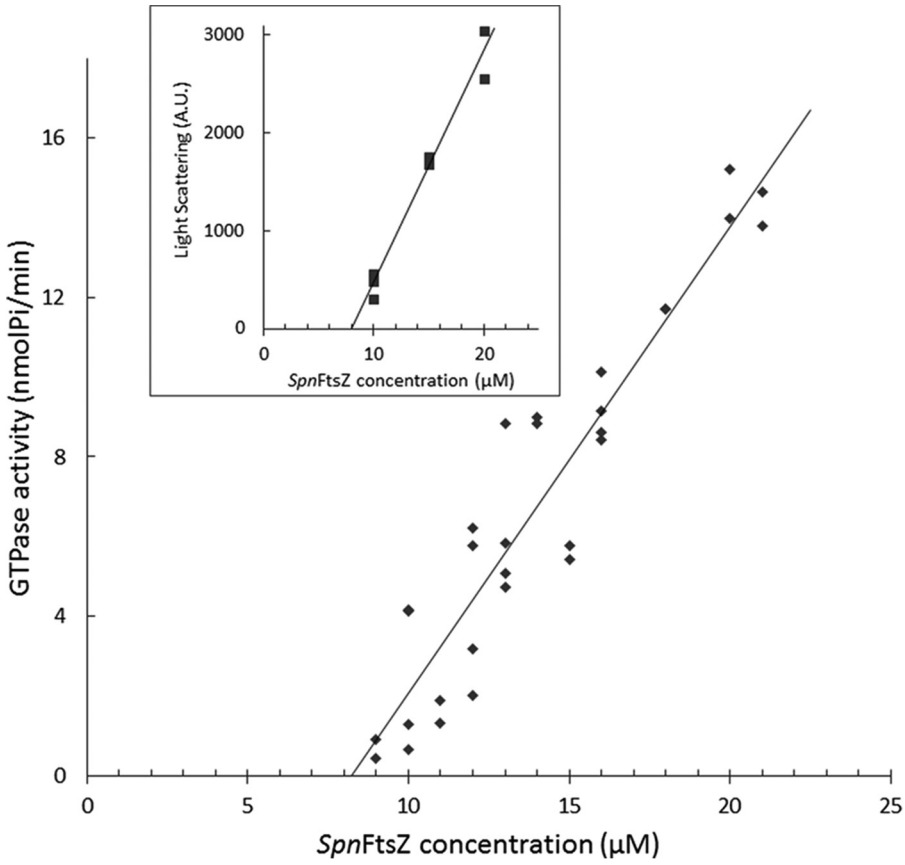

FIGURE 6. **Determination of *Spn*FtsZ critical concentration.** Velocities calculated from the slopes of the phosphate accumulation curves were semi-log plotted against *Spn*FtsZ concentrations ($p < 0.001$, $n = 30$ independent experiments). *Inset*, increments in 90° light scattering, calculated as the difference between the maximum value of the polymerization profile and the baseline without GTP (see Fig. 1), were semi-log plotted against protein concentrations ($p < 0.001$, $n = 9$ independent experiments).

FtsZ requires higher K^+ and Mg^{2+} concentrations than *Ec*FtsZ to reach maximal GTPase velocity values and Na^+ inhibited this activity.

The specificity for K^+ was also found in the GTP hydrolysis by *Mj*FtsZ (43, 49). When Na^+ is present, it competes with K^+ to occupy the catalytic GTPase active site and thus inhibits protein polymerization and GTP hydrolysis (48). Na^+ also inhibited *Spn*FtsZ polymerization detected in the light scattering assay (data not shown).

Critical Concentration of SpnFtsZ—To calculate the critical concentration of *Spn*FtsZ GTPase activity, velocities of GTP hydrolysis obtained in several experiments were plotted against protein concentrations (Fig. 6). Regression fitting indicated a critical *Spn*FtsZ concentration of 8 μM to hydrolyze GTP. In accordance, the degree of polymerization reached by different *Spn*FtsZ concentrations (10, 15, and 20 μM) analyzed by 90° light scattering assay (Fig. 1*A*) yielded the same critical concentration for *Spn*FtsZ assembly (Fig. 6, *inset*). Protein concentration dependence analyzed by sedimentation velocity supported these critical concentration calculations, because below 6 μM concentration no fast sedimenting species corresponding to FtsZ polymers were found, and most of the protein sediments as a polymer above 13 μM (Fig. 3). The critical concentration of *Spn*FtsZ observed in GTPase activity/polymerization assays is higher than values reported for other FtsZ proteins: 1 μM *Ec*FtsZ (14), 2 μM for *Mj*FtsZ (at pH 6.5) (43), 3 μM for *Mt*FtsZ (at pH 7.7) (50), and 4 μM for *Sa*FtsZ (at pH 6.5) (46).

Conclusion

We report the biochemical and biophysical characterization of the FtsZ from *S. pneumoniae*. The critical concentration, the delay observed in the GTPase activity, coupled to progressive elongation of the polymer, both strongly dependent on protein concentration, the well defined polymer size, and the tendency to form double-stranded filaments suggested a cooperative *Spn*FtsZ assembly mechanism. Our results for *Spn*FtsZ polymerization/GTPase activity provide evidence of the theoretical "intermediate" species in FtsZ polymerization dynamics suggested in different models of FtsZ polymerization that propose a FtsZ monomer nucleation step with conformational changes in the protein (21, 23, 25, 51). In the first minute after GTP addition (Fig. 7), *Spn*FtsZ scattered light, indicating the presence of polymers, but we detected no GTPase activity at 10 μM protein (at approximately the critical concentration). This effect on polymer development has not been reported for the *E. coli* protein. The slower kinetics and the higher critical concentration of *Spn*FtsZ allowed us to study the initial FtsZ polymerization/GTP hydrolysis reaction and to distinguish these two functions in the same polymer sample. Polymers shaped in the first minute of the reaction were large enough to produce strong light scattering but were unable to hydrolyze GTP detectably.

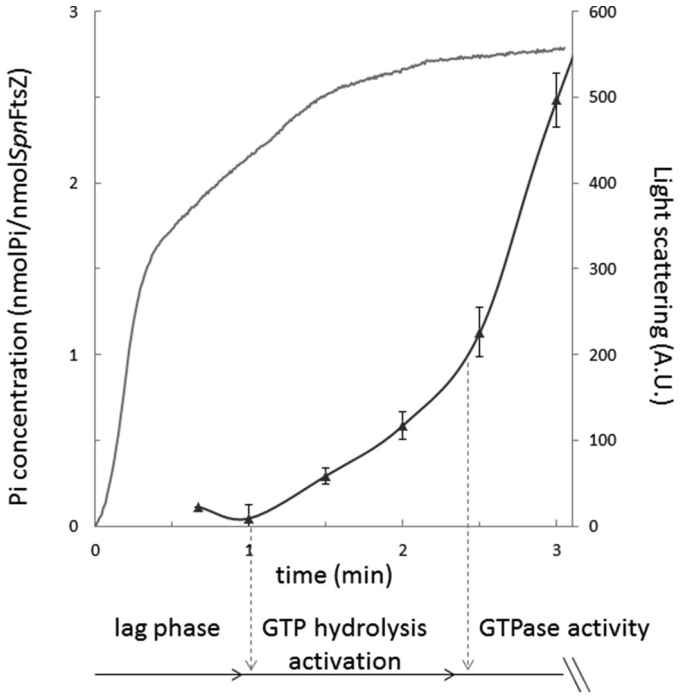

FIGURE 7. **The GTPase activity delay of *Spn*FtsZ.** At 10 μM protein, *Spn*FtsZ assembles at the onset of polymerization into polymers that scatter light but have no detectable GTPase activity (lag phase). Then shortly before maximum association, *Spn*FtsZ polymers begin to hydrolyze GTP in a transition reaction phase, whose duration is strongly dependent on protein concentration, to finally reach the full GTPase activity.

Although FtsZ polymers lacking GTPase activity have been obtained, including the FtsZW319Y-His6 mutant of *Mj*FtsZ (43), *Mt*FtsZ polymers at pH 6.5 (21), or *Ec*FtsZ polymers at pH 5.5 (48), no measurable transition of an inactive to an active polymer has yet been reported, although cooperative conformational transitions have been suggested in several models of FtsZ polymerization (25). Our data suggest that *Spn*FtsZ assembles through a cooperative mechanism that involves a nucleation step and a transition of the polymer from a GTPase inactive to active state.

Author Contributions—E. S., G. R., J. M., C. A., and A. I. R. designed the study and wrote the paper. E. S., M. K., P. G.-P., C. A., and A. I. R. performed research. All the authors analyzed the results and approved the final version of the manuscript.

Acknowledgments—We thank the personnel of the Proteomics and Genomics, Analytical Ultracentrifugation, and Electron Microscopy Facilities (Centro de Investigaciones Biológicas, Consejo Superior de Investigaciones Científicas) for help with Peptide Footprint, AUC, and EM experiments. We acknowledge the help of the CNB Electron Microscopy Service to obtain the EM image in Fig. 1 and Prof. Miguel Vicente for useful discussions.

References

1. Romberg, L., Simon, M., and Erickson, H. P. (2001) Polymerization of FtsZ, a bacterial homolog of tubulin: is assembly cooperative? *J. Biol. Chem.* **276,** 11743–11753
2. Mingorance, J., Rivas, G., Vélez, M., Gómez-Puertas, P., and Vicente, M. (2010) Strong FtsZ is with the force: mechanisms to constrict bacteria. *Trends Microbiol.* **18,** 348–356
3. Nogales, E., Downing, K. H., Amos, L. A., and Löwe, J. (1998) Tubulin and FtsZ form a distinct family of GTPases. *Nat. Struct. Biol.* **5,** 451–458
4. Biteen, J. S., Goley, E. D., Shapiro, L., and Moerner, W. E. (2012) Three-dimensional super-resolution imaging of the midplane protein FtsZ in live *Caulobacter crescentus* cells using astigmatism. *Chemphyschem* **13,** 1007–1012
5. Fu, G., Huang, T., Buss, J., Coltharp, C., Hensel, Z., and Xiao, J. (2010) *In vivo* structure of the *E. coli* FtsZ-ring revealed by photoactivated localization microscopy (PALM). *PLoS One* **5,** e12682
6. Li, Z., Trimble, M. J., Brun, Y. V., and Jensen, G. J. (2007) The structure of FtsZ filaments *in vivo* suggests a force-generating role in cell division. *EMBO J.* **26,** 4694–4708
7. Si, F., Busiek, K., Margolin, W., and Sun, S. X. (2013) Organization of FtsZ filaments in the bacterial division ring measured from polarized fluorescence microscopy. *Biophys. J.* **105,** 1976–1986
8. Rueda, S., Vicente, M., and Mingorance, J. (2003) Concentration and assembly of the division ring proteins FtsZ, FtsA, and ZipA during the *Escherichia coli* cell cycle. *J. Bacteriol.* **185,** 3344–3351
9. Stricker, J., Maddox, P., Salmon, E. D., and Erickson, H. P. (2002) Rapid assembly dynamics of the *Escherichia coli* FtsZ-ring demonstrated by fluorescence recovery after photobleaching. *Proc. Natl. Acad. Sci. U.S.A.* **99,** 3171–3175
10. Massidda, O., Nováková, L., and Vollmer, W. (2013) From models to pathogens: how much have we learned about *Streptococcus pneumoniae* cell division? *Environ. Microbiol.* **15,** 3133–3157
11. Natale, P., Pazos, M., and Vicente, M. (2013) The *Escherichia coli* divisome: born to divide. *Environ. Microbiol.* **15,** 3169–3182
12. Rico, A. I., Krupka, M., and Vicente, M. (2013) In the beginning, *Escherichia coli* assembled the proto-ring: an initial phase of division. *J. Biol. Chem.* **288,** 20830–20836
13. Jiménez, M., Martos, A., Vicente, M., and Rivas, G. (2011) Reconstitution and organization of *Escherichia coli* proto-ring elements (FtsZ and FtsA) inside giant unilamellar vesicles obtained from bacterial inner membranes. *J. Biol. Chem.* **286,** 11236–11241
14. González, J. M., Jiménez, M., Vélez, M., Mingorance, J., Andreu, J. M., Vicente, M., and Rivas, G. (2003) Essential cell division protein FtsZ assembles into one monomer-thick ribbons under conditions resembling the crowded intracellular environment. *J. Biol. Chem.* **278,** 37664–37671
15. Rivas, G., López, A., Mingorance, J., Ferrándiz, M. J., Zorrilla, S., Minton, A. P., Vicente, M., and Andreu, J. M. (2000) Magnesium-induced linear self-association of the FtsZ bacterial cell division protein monomer: the primary steps for FtsZ assembly. *J. Biol. Chem.* **275,** 11740–11749
16. Caplan, M. R., and Erickson, H. P. (2003) Apparent cooperative assembly of the bacterial cell division protein FtsZ demonstrated by isothermal titration calorimetry. *J. Biol. Chem.* **278,** 13784–13788
17. Chen, Y., Bjornson, K., Redick, S. D., and Erickson, H. P. (2005) A rapid fluorescence assay for FtsZ assembly indicates cooperative assembly with a dimer nucleus. *Biophys. J.* **88,** 505–514
18. González, J. M., Vélez, M., Jiménez, M., Alfonso, C., Schuck, P., Mingorance, J., Vicente, M., Minton, A. P., and Rivas, G. (2005) Cooperative behavior of *Escherichia coli* cell-division protein FtsZ assembly involves the preferential cyclization of long single-stranded fibrils. *Proc. Natl. Acad. Sci. U.S.A.* **102,** 1895–1900
19. Monterroso, B., Ahijado-Guzmán, R., Reija, B., Alfonso, C., Zorrilla, S., Minton, A. P., and Rivas, G. (2012) Mg^{2+}-linked self-assembly of FtsZ in the presence of GTP or a GTP analogue involves the concerted formation of a narrow size distribution of oligomeric species. *Biochemistry* **51,** 4541–4550
20. Mingorance, J., Rueda, S., Gómez-Puertas, P., Valencia, A., and Vicente, M. (2001) *Escherichia coli* FtsZ polymers contain mostly GTP and have a high nucleotide turnover. *Mol. Microbiol.* **41,** 83–91
21. Chen, Y., Anderson, D. E., Rajagopalan, M., and Erickson, H. P. (2007) Assembly dynamics of *Mycobacterium tuberculosis* FtsZ. *J. Biol. Chem.* **282,** 27736–27743
22. Huecas, S., and Andreu, J. M. (2003) Energetics of the cooperative assembly of cell division protein FtsZ and the nucleotide hydrolysis switch. *J. Biol. Chem.* **278,** 46146–46154
23. Huecas, S., Llorca, O., Boskovic, J., Martín-Benito, J., Valpuesta, J. M., and

Andreu, J. M. (2008) Energetics and geometry of FtsZ polymers: nucleated self-assembly of single protofilaments. *Biophys. J.* **94,** 1796–1806
24. Monterroso, B., Alfonso, C., Zorrilla, S., and Rivas, G. (2013) Combined analytical ultracentrifugation, light scattering and fluorescence spectroscopy studies on the functional associations of the bacterial division FtsZ protein. *Methods* **59,** 349–362
25. Miraldi, E. R., Thomas, P. J., and Romberg, L. (2008) Allosteric models for cooperative polymerization of linear polymers. *Biophys. J.* **95,** 2470–2486
26. Oliva, M. A., Trambaiolo, D., and Löwe, J. (2007) Structural insights into the conformational variability of FtsZ. *J. Mol. Biol.* **373,** 1229–1242
27. Natarajan, K., and Senapati, S. (2013) Probing the conformational flexibility of monomeric FtsZ in GTP-bound, GDP-bound, and nucleotide-free states. *Biochemistry* **52,** 3543–3551
28. Jamous, C., Basdevant, N., and Ha-Duong, T. (2014) Influence of GTP/GDP and magnesium ion on the solvated structure of the protein FtsZ: a molecular dynamics study. *J. Biomol. Struct. Dyn.* **32,** 916–927
29. Montecinos-Franjola, F., James, N. G., Concha-Marambio, L., Brunet, J. E., Lagos, R., Monasterio, O., and Jameson, D. M. (2014) Single tryptophan mutants of FtsZ: nucleotide binding/exchange and conformational transitions. *Biochim. Biophys. Acta* **1844,** 1193–1200
30. Monterroso, B., Rivas, G., and Minton, A. P. (2012) An equilibrium model for the Mg^{2+}-linked self-assembly of FtsZ in the presence of GTP or a GTP analogue. *Biochemistry* **51,** 6108–6113
31. Corton, J. C., Ward, J. E., Jr., and Lutkenhaus, J. (1987) Analysis of cell division gene *ftsZ* (*sulB*) from gram-negative and gram-positive bacteria. *J. Bacteriol.* **169,** 1–7
32. Lara, B., Rico, A. I., Petruzzelli, S., Santona, A., Dumas, J., Biton, J., Vicente, M., Mingorance, J., and Massidda, O. (2005) Cell division in cocci: localization and properties of the *Streptococcus pneumoniae* FtsA protein. *Mol. Microbiol.* **55,** 699–711
33. Fadda, D., Santona, A., D'Ulisse, V., Ghelardini, P., Ennas, M. G., Whalen, M. B., and Massidda, O. (2007) *Streptococcus pneumoniae* DivIVA: localization and interactions in a MinCD-free context. *J. Bacteriol.* **189,** 1288–1298
34. Sambrook, J., Fritsch, E. F., and Maniatis, T. (1989) *Molecular Cloning: A Laboratory Manual*, 2nd Ed., Cold Spring Harbor Laboratory, Cold Spring Harbor, NY
35. Ariza, A., Garzon, D., Abánades, D. R., de los Ríos, V., Vistoli, G., Torres, M. J., Carini, M., Aldini, G., and Pérez-Sala, D. (2012) Protein haptenation by amoxicillin: high resolution mass spectrometry analysis and identification of target proteins in serum. *J. Proteomics* **77,** 504–520
36. Ozols, J. (1990) Amino acid analysis. *Methods Enzymol.* **182,** 587–601
37. Small, E., and Addinall, S. G. (2003) Dynamic FtsZ polymerization is sensitive to the GTP to GDP ratio and can be maintained at steady state using a GTP-regeneration system. *Microbiology* **149,** 2235–2242
38. Schuck, P. (2000) Size-distribution analysis of macromolecules by sedimentation velocity ultracentrifugation and lamm equation modeling. *Biophys. J.* **78,** 1606–1619
39. Cole, J. L. (2004) Analysis of heterogeneous interactions. *Methods Enzymol.* **384,** 212–232
40. Geladopoulos, T. P., Sotiroudis, T. G., and Evangelopoulos, A. E. (1991) A malachite green colorimetric assay for protein phosphatase activity. *Anal. Biochem.* **192,** 112–116
41. Mukherjee, A., and Lutkenhaus, J. (1999) Analysis of FtsZ assembly by light scattering and determination of the role of divalent metal cations. *J. Bacteriol.* **181,** 823–832
42. Hernández-Rocamora, V. M., García-Montañés, C., Reija, B., Monterroso, B., Margolin, W., Alfonso, C., Zorrilla, S., and Rivas, G. (2013) MinC protein shortens FtsZ protofilaments by preferentially interacting with GDP-bound subunits. *J. Biol. Chem.* **288,** 24625–24635
43. Oliva, M. A., Huecas, S., Palacios, J. M., Martín-Benito, J., Valpuesta, J. M., and Andreu, J. M. (2003) Assembly of archaeal cell division protein FtsZ and a GTPase-inactive mutant into double-stranded filaments. *J. Biol. Chem.* **278,** 33562–33570
44. Ahijado-Guzmán, R., Alfonso, C., Reija, B., Salvarelli, E., Mingorance, J., Zorrilla, S., Monterroso, B., and Rivas, G. (2013) Control by potassium of the size distribution of *Escherichia coli* FtsZ polymers is independent of GTPase activity. *J. Biol. Chem.* **288,** 27358–27365
45. Martín-García, F., Salvarelli, E., Mendieta-Moreno, J. I., Vicente, M., Mingorance, J., Mendieta, J., and Gómez-Puertas, P. (2012) Molecular dynamics simulation of GTPase activity in polymers of the cell division protein FtsZ. *FEBS Lett.* **586,** 1236–1239
46. Elsen, N. L., Lu, J., Parthasarathy, G., Reid, J. C., Sharma, S., Soisson, S. M., and Lumb, K. J. (2012) Mechanism of action of the cell-division inhibitor PC190723: modulation of FtsZ assembly cooperativity. *J. Am. Chem. Soc.* **134,** 12342–12345
47. Salvarelli, E., Krupka, M., Rivas, G., Vicente, M., and Mingorance, J. (2011) Independence between GTPase active sites in the *Escherichia coli* cell division protein FtsZ. *FEBS Lett.* **585,** 3880–3883
48. Mendieta, J., Rico, A. I., López-Viñas, E., Vicente, M., Mingorance, J., and Gómez-Puertas, P. (2009) Structural and functional model for ionic (K^+/Na^+) and pH dependence of GTPase activity and polymerization of FtsZ, the prokaryotic ortholog of tubulin. *J. Mol. Biol.* **390,** 17–25
49. Oliva, M. A., Cordell, S. C., and Löwe, J. (2004) Structural insights into FtsZ protofilament formation. *Nat. Struct. Mol. Biol.* **11,** 1243–1250
50. Chen, Y., and Erickson, H. P. (2009) FtsZ filament dynamics at steady state: subunit exchange with and without nucleotide hydrolysis. *Biochemistry* **48,** 6664–6673
51. Chen, Y., and Erickson, H. P. (2005) Rapid *in vitro* assembly dynamics and subunit turnover of FtsZ demonstrated by fluorescence resonance energy transfer. *J. Biol. Chem.* **280,** 22549–22554

Microbiology:

The Cell Division Protein FtsZ from *Streptococcus pneumoniae* Exhibits a GTPase Activity Delay

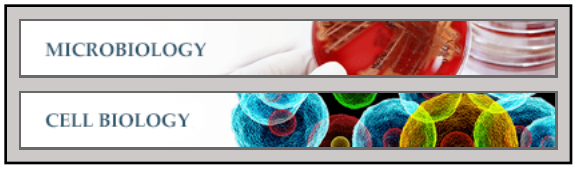

Estefanía Salvarelli, Marcin Krupka, Germán Rivas, Jesus Mingorance, Paulino Gómez-Puertas, Carlos Alfonso and Ana Isabel Rico

J. Biol. Chem. 2015, 290:25081-25089.
doi: 10.1074/jbc.M115.650077 originally published online September 1, 2015